Int J CARS (2017) 12:149–159
DOI 10.1007/s11548-016-1455-7

ORIGINAL ARTICLE

Robotic ultrasound-guided SBRT of the prostate: feasibility with respect to plan quality

Stefan Gerlach[1] · Ivo Kuhlemann[2] · Philipp Jauer[2] · Ralf Bruder[2] · Floris Ernst[2] · Christoph Fürweger[3] · Alexander Schlaefer[1]

Received: 13 January 2016 / Accepted: 29 June 2016 / Published online: 12 July 2016

Abstract
Purpose Advances in radiation therapy delivery systems have enabled motion compensated SBRT of the prostate. A remaining challenge is the integration of fast, non-ionizing volumetric imaging. Recently, robotic ultrasound has been proposed as an intra-fraction image modality. We study the impact of integrating a light-weight robotic arm carrying an ultrasound probe with the CyberKnife system. Particularly, we analyze the effect of different robot poses on the plan quality.
Methods A method to detect the collision of beams with the robot or the transducer was developed and integrated into our treatment planning system. A safety margin accounts for beam motion and uncertainties. Using strict dose bounds and the objective to maximize target coverage, we generated a total of 7650 treatment plans for five different prostate cases. For each case, ten different poses of the ultrasound robot and transducer were considered. The effect of different sets of beam source positions and different motion margins ranging from 5 to 50 mm was analyzed.
Results Compared to reference plans without the ultrasound robot, the coverage typically drops for all poses. Depending on the patient, the robot pose, and the motion margin, the reduction in coverage may be up to 50 % points. However, for all patient cases, there exist poses for which the loss in coverage was below 1 % point for motion margins of up to 20 mm. In general, there is a positive correlation between the number of treatment beams and the coverage.
Conclusion While the blocking of beam directions has a negative effect on the plan quality, the results indicate that a careful choice of the ultrasound robot's pose and a large solid angle covered by beam starting positions can offset this effect. Identifying robot poses that yield acceptable plan quality and allow for intra-fraction ultrasound image guidance, therefore, appears feasible.

Keywords SBRT · Image-guided radiation therapy · CyberKnife · Treatment planning · Ultrasound · Robotics

Introduction

Radiation therapy presents a non-invasive alternative for the treatment of prostate cancer. To balance the effectiveness of the irradiation against potential side effects, dose distributions conforming to the shape of the target and sparing critical structures, such as rectum and bladder, are preferable. Recently, this led to a number of approaches to leverage advances in the treatment systems to deliver more focused stereotactic body radiation therapy (SBRT) to the prostate [1,2].

However, a highly focused treatment also requires precise localization of the target. In general, to achieve the desired treatment effect, any uncertainty with respect to the clinical target volume (CTV) needs to be reflected by adding sufficient margins. Typical uncertainties, e.g., due to the setup, are accounted for by margins leading to the planning target volume (PTV). Similarly, systematic motion can be addressed by additional margins resulting in the internal target volume (ITV). As these margins enlarge the treated volume, high doses will affect normal or critical structures in the proxim-

✉ Alexander Schlaefer
schlaefer@tuhh.de

1 Institute of Medical Technology, Hamburg University of Technology, Hamburg, Germany

2 Institute for Robotics and Cognitive Systems, Universität zu Lübeck, Lübeck, Germany

3 Europäisches Cyberknife Zentrum München-Großhadern, Munich, Germany

ity of the CTV. This can be mitigated using smaller margins if information on the target motion can be obtained during treatment and the treatment is adjusted. The idea to track the target motion and move the beams accordingly was first implemented for the robotic CyberKnife (Accuray Inc., Sunnyvale) [3]. Other motion compensation approaches based on multileaf collimators (MLC) [4,5], the treatment couch [6,7], or the VERO system (VERO GmbH, Germany) [8] have also been studied.

One key challenge for active motion compensation is sufficiently fast tracking of the internal motion. A typical approach uses artificial landmarks, either as active transponders [9,10] or gold fiducials localized with X-ray imaging. Ideally, tracking would allow localizing the whole target without the need to implant fiducial markers. However, continuous fluoroscopic X-ray imaging is not feasible for prolonged treatments and the soft-tissue contrast in the abdomen is poor. This resulted in a recent interest in integrating magnetic resonance imaging (MRI) with beam delivery devices [11–13]. Another alternative is fast volumetric ultrasound (US), for which volume rates of more than 20 Hz have been reported and recent work has shown that motion tracking is possible [14–16]. Despite the high spatial and temporal resolution and a history in radiation therapy setup [17,18], the integration of ultrasound with external radiation therapy devices remains difficult. One limitation is the need to carefully and continuously position the probe on the patient to realize good image quality. Therefore, a number of approaches for robotic ultrasound placement have been studied [15,16,19,20]. Clearly, such an ultrasound robot needs to maintain the imaging position, while any risk for the patient or collisions with other system components must be avoided.

Another limitation is the blocking of beams by the ultrasound transducer and the robotic arm holding it. In general, the problem to find the optimal beam arrangement for radiation therapy is complex, and no analytical solution is known. Conventional coplanar treatments often use pre-defined beam geometries, e.g., of five-to-nine different directions [21,22], but non-coplanar beam arrangements can result in substantial further improvements. This is particularly interesting for complex cases, where plan quality metrics include a number of conflicting criteria, such as superior dose coverage, high conformality and steep dose gradients, and a practical treatment time. Hence, limiting the available beam directions can have a clear adverse effect on the plan quality for non-coplanar treatments [23]. Interestingly, initial results provided by Schlosser et al. [16] for their ultrasound robot illustrate the problem: even for a seven-beam prostate setup, the coverage of the original planning target volume dropped by more than 10 %. While the authors did not focus on a plan quality analysis, precise and focalized delivery of a conformal dose distribution is one key aspect of stereotactic body radiation therapy (SBRT). Hence, ultrasound-based tracking should not compromise the plan quality. We present an analysis of ultrasound probe placement using a light-weight arm commercially available. Considering the flexibility of CyberKnife beam placement, we study the impact of different robot poses on the beam generation and the plan quality. Our results indicate that the blocking of beams can have a substantial impact on the plan quality but that careful selection of the ultrasound robot pose will mitigate these effects.

Material and methods

Ultrasound robot

While different kinematics for positioning ultrasound probes have been proposed, the robot will need to be sufficiently small and lightweight to be integrated with the delivery system, while at the same time, it needs to be stiff enough to press and hold the ultrasound transducer at the abdominal wall for good image quality. Moreover, the robot needs to be designed for direct interaction with the patient. We consider a light-weight robot (KUKA LBR iiwa) which is available in a 'medical assistant' version and certified for use in human–robot collaboration. Another interesting feature is a seventh joint, which makes the robot kinematically redundant. This means the robot can reach the same pose with different configurations, e.g., the ultrasound transducer remains at the same position, while the robots elbow can be moved to avoid the treatment beam. A possible setup is shown in Fig. 1a.

In the image guidance scenario, the robot carries an ultrasound transducer. Recently, fast ultrasound imaging with volume rates facilitating motion compensation has been demonstrated [14,15]. We consider the same 2D array transducer (GE 3V, GE Healthcare) in our study. For the robot, we use a shape model for which we establish the pose using the actual forward kinematics. The location of the robot's base with respect to the patient is another degree of freedom. For the planning experiments, we considered two cases. In the first case, it is positioned to the right-hand side of the patient and in longitudinal position close to the prostate's centroid. In the second case, the base is placed inferior of the perineum.

Clearly, to realize image guidance the transducer needs to have a clear field of view towards the prostate. Typically, promising positions are on the abdominal wall, which means the robot and transducer would interfere with the beams targeted at the prostate. Hence, different beams would be blocked for different poses. To study the effect of the robot pose on the plan quality, we have selected the ten poses and robot configurations shown in Fig. 2. When selecting these poses, we considered results of a viewport analysis [19], which highlights continuous areas with expected good visibility of the target structures in red, and further areas with visibility of the target in blue (see Fig. 1b). The first

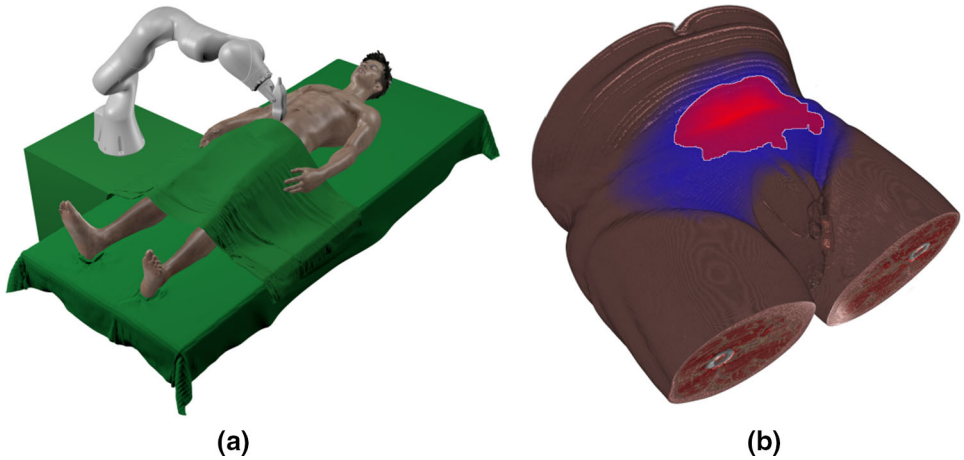

Fig. 1 **a** Illustration of the general setup with a light-weight robotic arm positioning the ultrasound probe. **b** The figure highlights the ideal (*red*) and possible (*blue*) viewports for the ultrasound probe

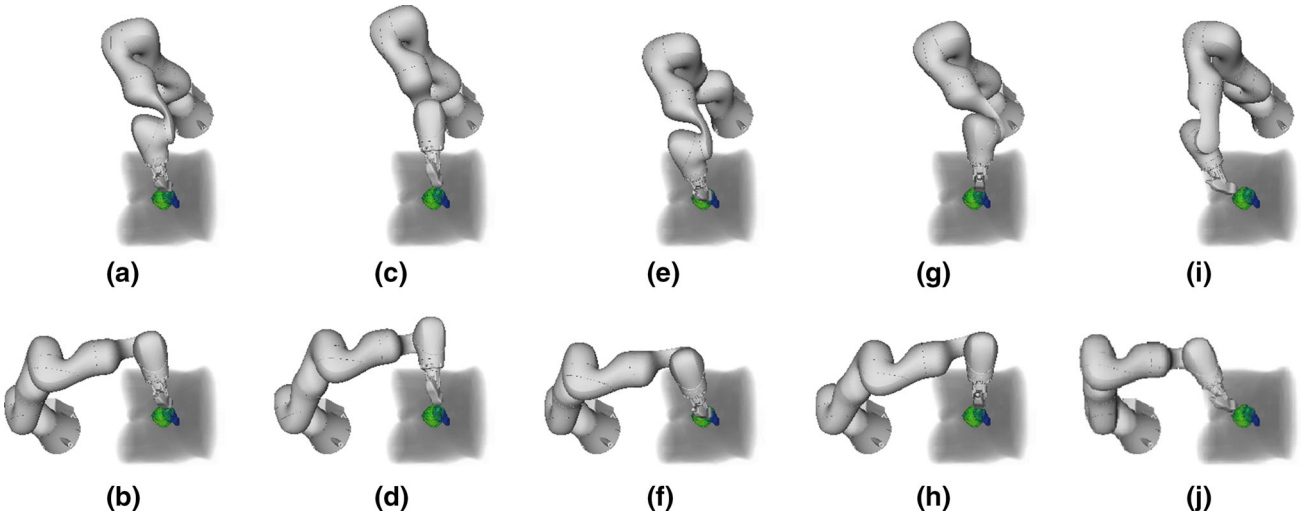

Fig. 2 Ten ultrasound robot poses (**a** = pose 1 through j = pose 10) studied in the experimental analysis. Pose 1 **a** places the transducer approximately at the center of the ideal viewport shown in Fig. 1b, while the other poses represent placements closer to the fringe of the potential viewport. Note that the ultrasound transducer poses 2, 4, 6, 8, 10 are the same as poses 1, 3, 5, 7, 9, however, the robot's base is in a different positions with respect to the patient

selected pose (pose 1) reflects a case, where the transducer is positioned anterior and slightly superior of the prostate, approximately at the center of the red area in Fig. 1b. In pose 3, the transducer is tilted to the right, and in pose 5, it is tilted to the left. Likewise, the transducer is tilted in superior and inferior direction for poses 7 and 9, respectively. Poses 2, 4, 6, 8, and 10 realize the same transducer placements for the second position of the robot's base.

Beam generation

We study the integration of ultrasound tracking with the robotic CyberKnife, which allows for a flexible beam positioning. During treatment, the robot mounted linear accelerator is placed at a number of discrete points called beam nodes. From each node, beams with different orientations can be delivered. We consider beams with a circular cross section, as created by the widely used cylinder and IRIS collimators [24].

Typically, beams are generated in a heuristic fashion [25] connecting beam nodes to points inside the PTV. However, in the presence of the ultrasound robot not all such beams are feasible, as they should not pass through the robot or the transducer. Moreover, the purpose of ultrasound image guidance is to detect target motion, which is then compensated by respective beam motion.

As this motion may move the beam towards the ultrasound robot, it also has to be considered during planning.

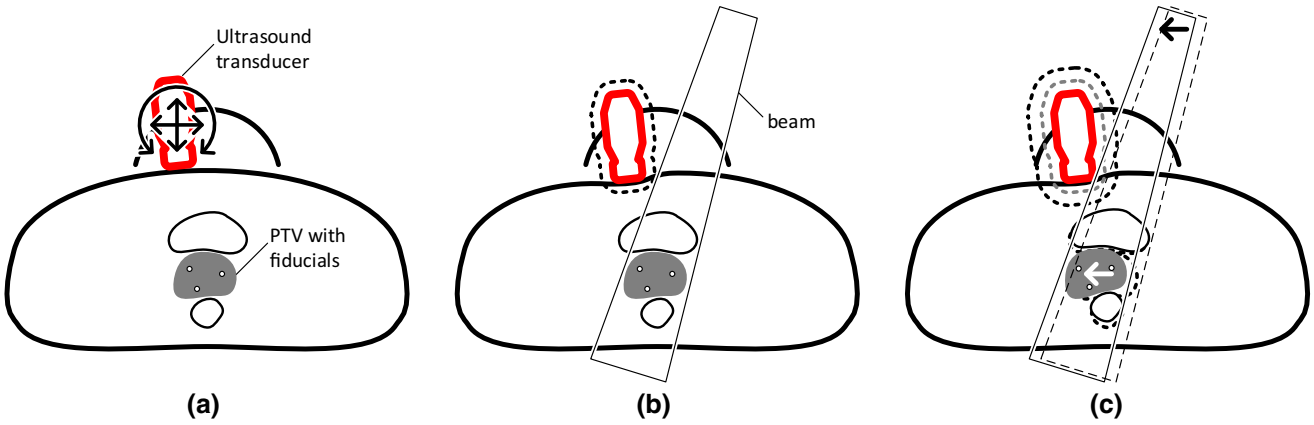

Fig. 3 Prostate geometry with white landmarks in the *gray* PTV. **a** While promising ultrasound transducer positions can be established during planning, additional small translations and rotations will be required to obtain good image quality. **b** During planning, this transducer motion can be considered by a safety margin (*dotted black line*). The beams will be computed based on the static planning CT. **c** When the PTV moves during treatment, the beams will move accordingly. To account for this motion, a second safety margin is introduced (*dotted black line* around the transducer)

Figure 3 shows the need for safety margins. In the planning scenario, we have to assume a transducer position based on the viewport estimation (compare Fig. 1b). To achieve and maintain good image quality of the target region, small additional translation and rotation of the transducer will be required during the actual setup and throughout the treatment. This motivates placing the transducer on the abdominal wall and adding a first safety margin, as shown in Fig. 3b. During motion compensated treatment, the beams may follow the target motion towards the transducer, and hence Fig. 3c shows that an additional motion margin should account for this motion. In this study, we consider the effect of different margins on the plan quality.

We determine a set of feasible beams in the following fashion. First, for each node n, we compute the projection of ultrasound robot and transducer to a plane p that is normal to the line connecting n and the centroid of the PTV. Second, we compute the distance transform for the projection. Third, we generate potential beams using the conventional and clinically proven heuristic. For each potential beam, the effective radius r in the plane p as well as the point p_i, where the beam's centerline intersects p are computed. Using the distance transform, we can establish whether the distance of p_i to the projection of robot and transducer is smaller than r. In this case, the beam is discarded; otherwise, it is included in the set of candidate beams considered for treatment planning. Figure 4 shows the approach and the resulting reduction in the number of beams. Note that for some nodes, there are beams that can be delivered and other beams that cannot be delivered.

Clearly, the plan quality will depend on the number of nodes and beams considered in the discrete plan optimization problem. Typically, up to 140 nodes are used, with the actual number available in a specific patient case depending on further restrictions, e.g., the complete radiological path from skin surface to target being visible in the computer tomography (CT) image. Hence, the actual node set for different patients varies. To account for this, we obtained treatment plans for the original node set per patient (node set "0"), a union of all node sets of the considered patients (node set "1"), and an artificial node set with 25 nodes equidistantly sampled around the patient (node set "2").

Plan optimization

We use a stepwise optimization approach based on linear programming [26] which is similar to the clinically implemented planning method. One particular advantage is the use of hard constraints on all dose bounds, except for the bound that represents the objective of the current optimization step. For comparability, we maintain the exact same bounds on the OAR for all patient cases and planning scenarios. The objective is to maximize the coverage of the PTV, which is realized as minimizing the sum of slack variables measuring the dose deviation from the desired prescribed dose. After optimization, the set of candidate beams is effectively partitioned in beams with zero activation time and beams with non-zero activation time. The latter beams form the actual treatment beams.

Patient data and experimental scenarios

We studied five prostate patient data sets previously treated with the CyberKnife. The PTVs had a volume of 67135, 93219, 82301, 81111, and 70277 mm^3, i.e., reflecting a range of typical target sizes. The CT image, the contours, the beam

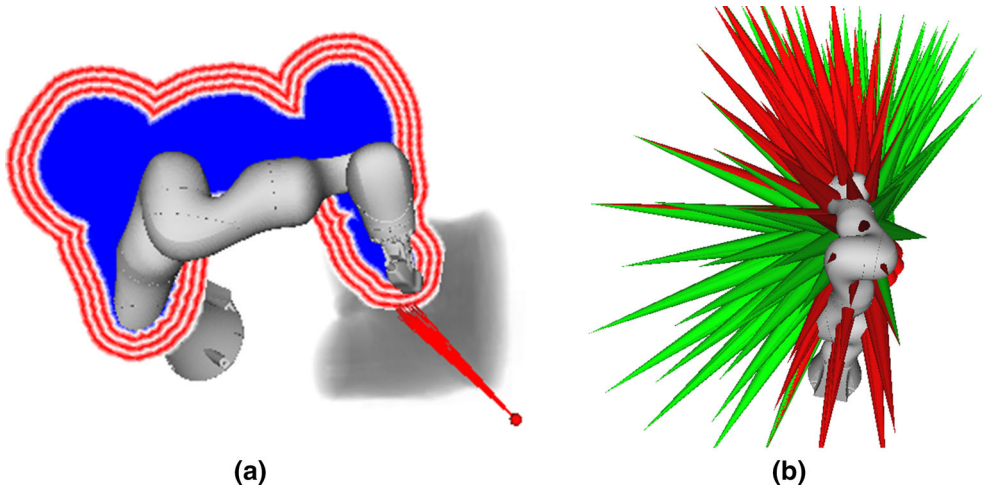

Fig. 4 **a** Illustration of the test for intersection of beams and ultrasound robot. A plane running through the PTV is *colored blue*, where all beams from the given node intersect with the robot. The *red lines* denote the 20, 40, and 60 mm margin, respectively. **b** Illustration of the effect on the beam set, the *red beams* are removed from the candidate beam set. For some nodes, some beams are deliverable while other beams are not

nodes and treatment beams, and the physics data underlying the dose calculations were imported into our planning system. To achieve a comparable starting point, we considered the PTV, the rectum, the bladder, and two SHELL structures to maintain a conformal dose distribution. Different approaches for prostate SBRT have been proposed [1]. We used dose bounds adapted from a five fraction protocol with a prescribed dose of 36.25 Gy and dose-volume constraints for the OARs. We required stricter upper dose bounds for rectum and bladder, while we relaxed the upper bound of the PTV to approximately 120 %. Primarily, this allows to maintain a fix (and relatively low) bound on the total monitor units for all five patients, which is set to 25,000. Another motivation is that there are protocols allowing for a much more pronounced dose escalation in the PTV [2]. The two SHELLs at 3 and 18 mm distance and with bounds of 36 and 22 Gy, respectively, yield a conformal dose distribution.

In a first scenario, we considered the effect of the different robot poses on the resulting plan quality, compare Fig. 2. In addition, we also studied the effect of different safety margins on the plan quality. Here, the safety margin refers to an additional distance between beam and ultrasound robot projection to account for the potential movements of the transducer and the beam motion. We considered margins of 5, 10, 20, 35, and 50 mm. Finally, we also analyzed the effect of the different node sets to address the question whether beams from fewer nodes can result in acceptable plan quality. In our current analysis, we kept the number of candidate beams constant at 4000, and hence, each of the fewer nodes carries more candidate beams. Given that the beam generation heuristics include randomness, all experiments were repeated ten times for different random seeds.

Results

The change in coverage due to the different poses blocking beams is presented in Fig. 5. Figure 5a shows that the PTV coverage drops depending on the pose, with the most notable difference for pose 1. Figure 5b, c shows that the dose to rectum and bladder is well below the upper bounds defined by a typical protocol. Moreover, the maximum and higher doses are very similar for all plans, i.e., there was no compromise with respect to OAR sparing. The reduction in coverage is more pronounced for larger safety margins, as shown in Fig. 6, for pose 1 and summarized for all poses and margins in Fig. 7. Figure 7c also shows that the loss in coverage is less severe for fewer nodes.

The key results for all patient cases are summarized in Fig. 8, which shows the best and worst coverages for each plan and each margin. The figure illustrates that the general loss in coverage due to the robot blocking nodes is visible for all patients. Particularly, poses 9 and 10 always show a substantial drop in coverage compared to the reference plan and often present the worst choice. Throughout the five patients, the best coverage is most often achieved for pose 7.

Figure 9 shows the actual blocking of nodes for patient 1, pose 1, and a 20 mm margin. Nodes colored in red are completely blocked, i.e., no beam is delivered from theses nodes. Nodes colored in yellow have some beams removed and some delivered, while green nodes have no beams removed. In Fig. 10, the overall relationship of coverage and number of weighted beams and nodes is shown. Note that the figure contains values for all plans and that the reference plans use most nodes.

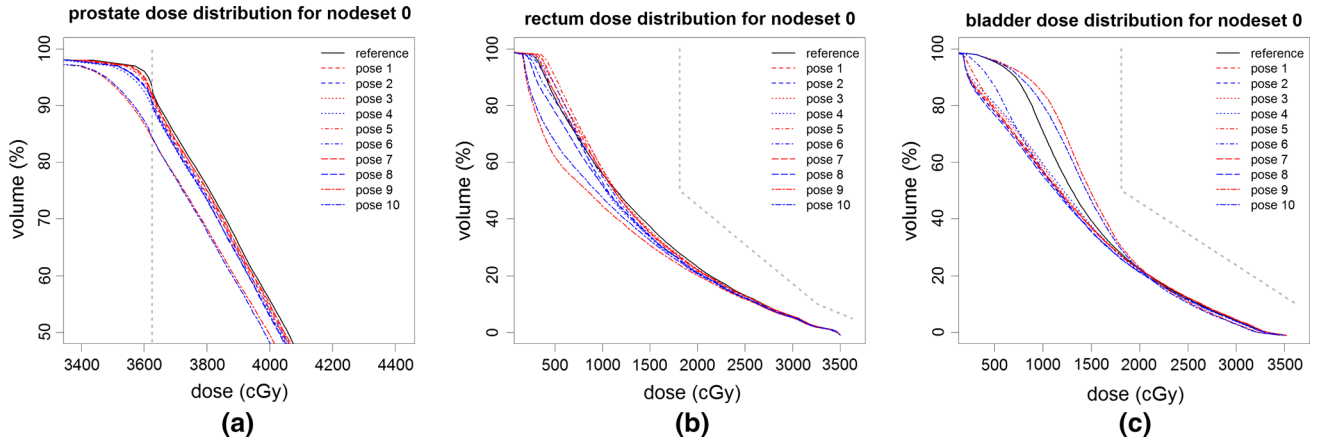

Fig. 5 Dose distribution in the PTV, the rectum, and the bladder, for the reference (*gray*), and the ten poses, respectively, all for patient case 1. The plots represent mean values and the safety margin was 20 mm. Both OAR remain clearly below the dose-volume constraints represented by the *dotted gray lines*

Table 1 gives the differences in coverage between the reference plan and the poses with the maximum and minimum coverages, respectively. The last two columns contain the maximum of the maximum and minimum differences over all five plans. For example, for margins up to 20 mm, there exists a pose for each patient, such that the coverage reduces <1 % point.

Table 2 further summarizes the change in coverage for the three different node sets. Particularly, the table also gives the mean number of beams and nodes used in the respective plans, which is typically smaller for the scenarios, including the ultrasound robot. Table 3 presents results for pose 1 and different margins. The number of beams and nodes included in the plans is lower for larger safety margins. The correlation between coverage and the number of beams and nodes is summarized in Table 4. For all patients and node sets "0" and "1", there is a correlation between the number of beams and the coverage. The correlation between the number of nodes and the coverage depends on the patient, but it is generally rather weak.

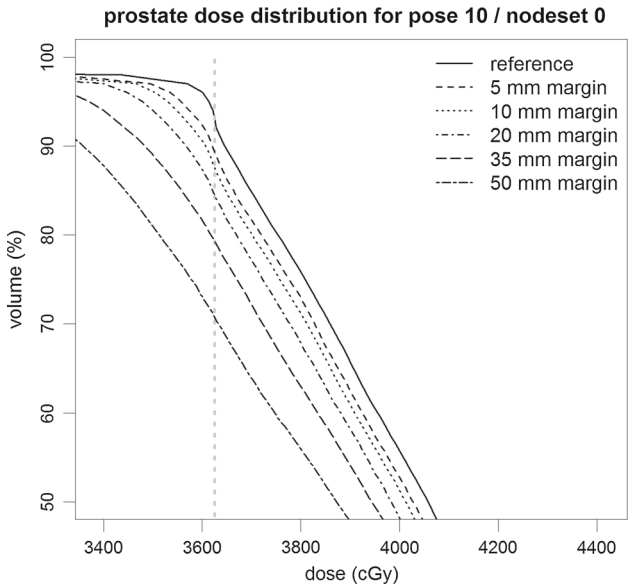

Fig. 6 Dose distribution in the PTV for the reference (*solid*) and the five margins and pose 10, respectively, all for patient case 1. The DVH plots represent mean values over ten different random candidate beam sets

Discussion

The results show that the robotic placement of an ultrasound probe will block beams from certain directions, which in turn typically results in a degraded plan quality. This general pattern can be seen for all patients, most robot poses, and all safety margins. As shown in Fig. 5, other plan quality parameters are maintained by the imposed bounds and the observed effects are, therefore, related to the ultrasound robot.

However, the results also indicate that different transducer poses lead to substantially different plan quality. This is highlighted by Fig. 8, which shows that for some transducer poses, the change in coverage is small, while other poses cause a substantial reduction in coverage. Moreover, the best pose depends on the patient case and the margin. Hence, a careful selection of the ultrasound transducer and robot pose could mitigate the negative impact on plan quality. This is also supported by Table 1, which gives the maximum and minimum changes in coverage for each patient. Particularly, the table shows that the maximum reduction in coverage over the best poses of all five patients is below 1 % point for up to 20 mm margins. Note that in our current study, we have included only five different transducer poses and there may be room for further optimization of the transducer and robot poses.

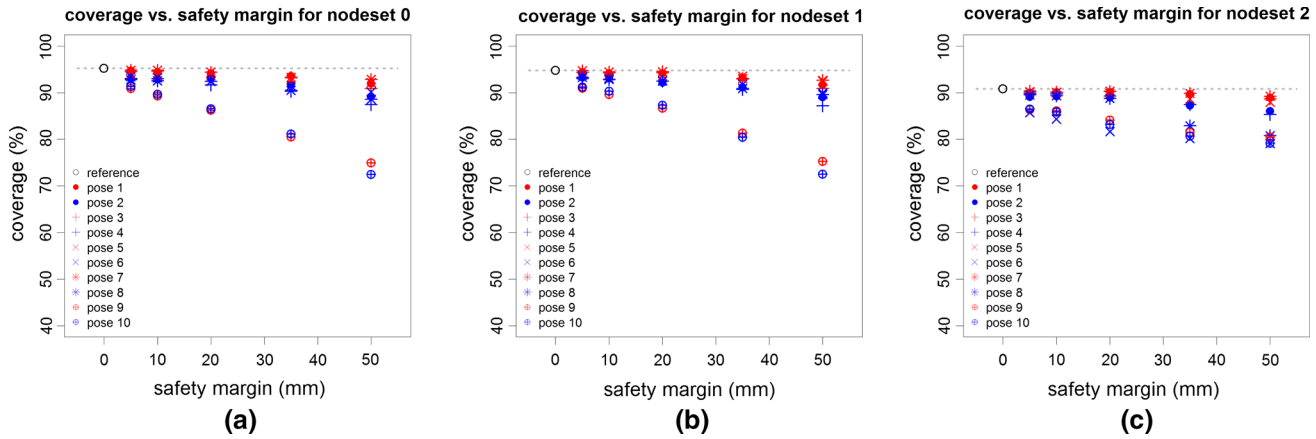

Fig. 7 Coverage with respect to different safety margins and the different poses, and the three different node sets, all for patient case 1. The values represent the mean values over all ten runs

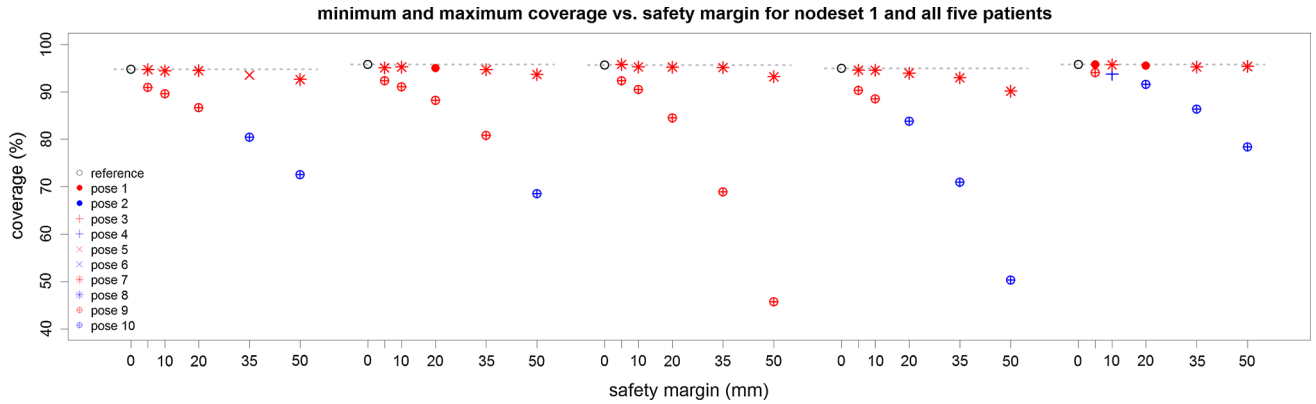

Fig. 8 Minimum and maximum coverages for the joint node set (node set "1") with respect to the five plans (*left to right*), different safety margins, and the different poses. The values represent the mean values over all ten runs

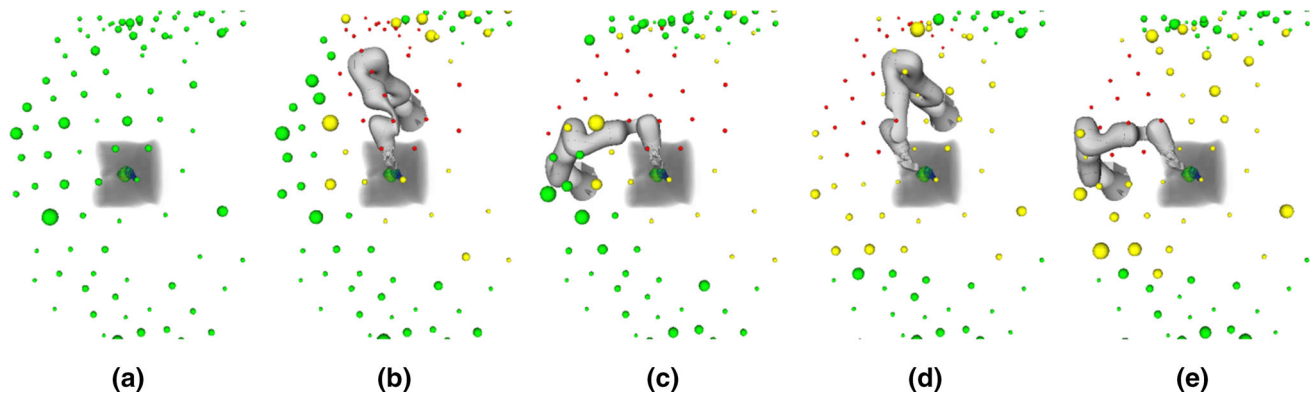

Fig. 9 Comparison of the nodes available for dose delivery. *Green*, *yellow*, and *red spheres* denote nodes where all, some, and no beams could be delivered, respectively. The size of the spheres corresponds to the number of beams delivered from the respective node. Subfigures **a**–**e** show results for patient 1 and the reference plan, pose 1, pose 2, pose 9, and pose 10, respectively

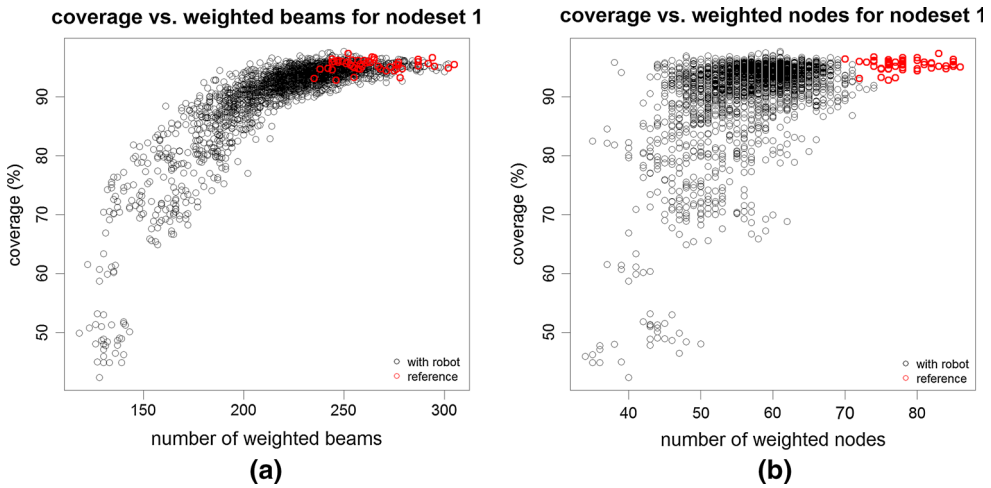

Fig. 10 Coverage with respect to **a** the number of weighted beams and **b** the number of weighted nodes for node set "1" and all five cases. *Red circles* denote the reference plans

Table 1 Maximum and minimum decrease in coverage over the ten poses, both with respect to the reference plan and node set "1" and given in percentage points. The last two columns give the respective maxima with over all patients. Note that the apparent improvements are due to the randomized beam generation and different subsets of the node set available for different poses and margins

Margin	Patient 1		Patient 2		Patient 3		Patient 4		Patient 5		over all patients	
	Max	Min	Max	Min	Max	Min	Max	Min	Max	Min	Max max	Max min
5 mm	3.82	0.05	3.40	0.70	3.33	−0.13	4.60	0.34	1.72	0.04	4.60	0.70
10 mm	5.18	0.31	4.74	0.53	5.15	0.35	6.40	0.34	2.06	0.10	6.40	0.53
20 mm	8.11	0.27	7.55	0.76	11.17	0.41	11.15	0.97	4.21	0.26	11.17	0.97
35 mm	14.35	1.23	15.00	1.08	26.78	0.49	24.05	1.95	9.46	0.54	26.78	1.95
50 mm	22.27	2.13	27.28	2.10	49.92	2.44	44.59	4.79	17.43	0.43	49.92	4.79

Table 2 Basic statistics for coverage, number of weighted beams, and number of weighted nodes for the reference plans and the plans for the different poses, different node sets, and a margin of 20 mm. All results are with respect to the 5 cases and 10 runs with different random seeds

Scenario	Node set 0						Node set 1						Node set 2					
	Cov. (%)		Beams		Nodes		Cov (%)		Beams		Nodes		Cov. (%)		Beams		Nodes	
	μ	σ	μ	σ	μ	σ	μ	σ	μ	σ	μ	σ	μ	σ	μ	σ	μ	σ
Reference	95.7	0.9	265	16	70	3.1	95.4	0.9	264	17	78	3.9	93.4	1.9	249	19	24	0.9
Pose 1	94.5	1.3	245	14	52	2.8	94.7	1.1	248	13	55	2.4	91.9	1.8	231	16	20	0.8
Pose 2	93.3	1.5	228	16	56	2.6	93.3	1.4	227	13	60	2.7	90.3	1.6	219	12	21	0.8
Pose 3	94.1	1.2	245	13	54	2.9	94.1	1.1	242	13	57	2.3	91.7	1.8	229	15	19	1.2
Pose 4	91.0	2.4	212	15	54	4.0	91.9	1.7	219	11	58	2.7	90.9	1.9	223	15	21	0.9
Pose 5	94.4	1.3	241	15	51	3.1	94.4	1.2	246	12	55	2.4	91.6	1.6	227	15	20	1.2
Pose 6	93.8	1.4	229	17	56	2.9	93.9	1.2	231	13	62	2.4	84.8	3.2	211	12	22	0.9
Pose 7	94.8	1.2	251	16	54	2.7	94.8	1.1	255	17	58	2.6	92.4	2.0	235	19	20	0.7
Pose 8	93.6	1.4	231	19	55	2.9	93.6	1.3	233	16	59	2.7	90.2	2.3	222	16	21	1.0
Pose 9	86.3	3.1	181	17	51	4.6	87.0	3.3	189	15	55	4.0	86.6	2.9	207	13	20	0.7
Pose 10	87.8	3.1	190	19	56	4.8	87.8	2.9	191	16	62	4.6	85.4	2.9	210	13	22	0.7

In general, more weighted nodes and beams correspond to better coverage, which is the figure of merit in our scenario. Yet, Fig. 10 also shows that good results with acceptable coverage are feasible for substantially lower numbers of weighted beams and nodes. Particularly, Fig. 10b indicates that there is some redundancy with respect to the set of nodes. This is also supported by Fig. 9, where some nodes contribute more to the dose delivery than other nodes, even in the reference scenario. Blocking these "preferable" nodes seems to be related to a particular drop in coverage. For example, consider Table 2 for a 20 mm margin and the original patient node set (node set "0"). The mean reference coverage is 95.7 % with the dose delivered by 265 beams from 70 nodes. For pose 1, the mean coverage remains comparable at 94.5 % with 245 beams but only 52 nodes used. In contrast, the coverage for pose nine drops to 86.3 % with 181 beams delivered from 51 nodes.

The relationship between the coverage and the number of beams and nodes is also reflected in Table 3, which details how the coverage decreases for increased safety margins and pose 10. While there are fewer nodes used in the plans, it seems that particularly the reduced number of active beams impacts the plan quality. This hypothesis is also supported by Table 4, which shows the correlation between coverage and number of beams and nodes for the different patients and node sets. Interestingly, the coverage for node set "2" seems less dependent on the number of beams and nodes. This can be explained by the sparse nature of this node set, which uses just 25 nodes and covers a large solid angle around the patient. Hence, unless the margin is increased substantially, only few nodes are blocked. Note that the reference coverage is lower than for the other node sets, indicating that more than 25 beam directions should be considered.

As we keep the number of candidate beams constant, a larger number of nodes results in fewer candidate beams per node, i.e., fewer beams to choose from this particular direction. This issue cannot be easily avoided, as both the number of nodes and the number of beams affect the plan quality. In general, the results indicate that using the flexibility of robotic beam delivery can offset the effect of integrating the ultrasound robot. This motivates a careful optimization of the robot's pose and the beam directions, with additional beams added to unblocked and promising directions. It must be noted, however, that the resulting optimization problem adds another combinatorial layer to the already difficult beam orientation problem. Furthermore, it would also be interesting to study an enlarged set of beam nodes, i.e., covering more lateral and posterior beam directions when the ultrasound robot is considered [23].

A general remark must be made with respect to the absolute value of the coverage we have obtained. The parameters were chosen to obtain realistic reference plans with a PTV coverage of approximately 95 %, which would be typical after prescription. In our scenario, the strict upper bound constraints on the total monitor units and on the dose in both SHELL structures, the PTV, and the rectum are active. Hence, for a fix bound on the monitor units, the tradeoff is primarily between coverage and conformality. Given the multi-objective nature of the treatment planning problem, any of the strict bounds we maintained could be relaxed to improve the coverage [26]. Clearly, in our analysis, we wanted to avoid such effects. However, particularly, the bound on the total monitor units presents a good candidate for a tradeoff.

Another interesting question regards the right choice of the safety margin. Clearly, if planning is done before the actual treatment fraction, all motion of the transducer has to be anticipated. We expect that a force controlled placement of the transducer will be possible within 10–20 mm motion from the planned pose. Further work needs to analyze the typical motion needed to re-position the transducer during a full treatment fraction, e.g., due to movements of the patient and the abdominal wall. The actual motion of the beams also needs to be studied further. However, recent work indicates that a 10 mm margin may also be appropriate, e.g., the motion was reported to typically be within 6, 6, and 4 mm

Table 3 Basic statistics for coverage, number of weighted beams, and number of weighted nodes for the reference plans and the plans for the different margins, pose 10 and node set "0"

Scenario	Cov. (%)		Beams		Nodes	
	Mean	sd	Mean	sd	Mean	sd
Reference	95.7	0.9	265	16.1	70	3.1
5 mm	92.7	1.5	213	18.6	60	4.1
10 mm	91.2	2.0	206	17.2	59	4.3
20 mm	87.8	3.1	190	19.3	56	4.8
35 mm	78.6	6.2	165	19.2	52	4.9
50 mm	64.2	11.3	145	17.0	48	6.5

Table 4 Correlation between coverage and the number of beams and the number of nodes for different patients and node sets, respectively

Patient	1			2			3			4			5		
Node set	0	1	2	0	1	2	0	1	2	0	1	2	0	1	2
Cor #beams	0.84	0.86	0.59	0.86	0.87	0.63	0.87	0.87	0.81	0.87	0.87	0.65	0.87	0.86	0.60
cor #nodes	0.25	0.29	−0.20	0.25	0.21	−0.01	0.60	0.68	0.41	0.63	0.57	0.22	0.47	0.34	0.07

along the superior–inferior, anterior–posterior, and left–right axes [27]. It should be noted that the pose of both robots is known throughout treatment, and hence, a possible collision of the beams with the ultrasound imaging subsystem can be detected before the respective motion occurs, i.e., the treatment would be stopped to repeat setup. Hence, the margin also represents a tradeoff with respect to blocking beams and nodes and the likelihood of interrupting the beam delivery.

So far, proposals to integrate ultrasound image guidance with radiation therapy have focused on conventional LINAC-based treatment systems [16,28]. Particularly for IMRT prostate treatments, the impact of the transducer can be substantial, as the delivery of beams through the transducer should be avoided [29]. Interestingly, this also led to a recent approach to reduce the radio-opacity of the transducer by moving electronics and metal parts further away [30]. This may be promising for the coplanar beam delivery typical with LINACs. However, our results illustrate that the larger flexibility of beam placement with the CyberKnife can be used to mitigate the impact of the transducer. Moreover, using a kinematically redundant robot, the configuration of the robot and the pose of the transducer can be changed throughout treatment. The optimal placement of robot and transducer may be counterintuitive, e.g., in our study, a lateral position of the robot outperforms a robot placement between the patient's legs. Therefore, treatment plan optimization methods accounting for robot and transducer probe need to be considered.

Conclusion

Robotic ultrasound imaging may be a viable alternative to realize fast, volumetric imaging during SBRT. This would be particularly interesting for treatment regimens using high doses and steep gradients with respect to surrounding and critical structures. We demonstrate that placing an ultrasound robot into a CyberKnife prostate treatment scenario may lead to a reduction in the achievable plan quality. However, the benefit of non-invasive and non-ionizing tracking of organ motion and deformation in the abdomen throughout beam delivery may outweigh the loss in coverage, particularly as it may allow tighter margins. Moreover, our results indicate that a careful optimization of the ultrasound robot pose and position can mitigate its effect on the treatment.

Compliance with ethical standards

Funding This study was partially funded by Deutsche Forschungsgemeinschaft (Grants ER 817/1-1 and SCHL 1844/3-1).

Conflict of interest Ralf Bruder is co-inventor of a patent pending method for positioning an ultrasound transducer. Floris Ernst has received Grants from Varian Medical Systems, Inc. The other authors declare no conflict of interest.

Ethical approval This article is based on fully anonymized treatment planning data and does not contain any studies with human participants or animals performed by any of the authors.

Informed consent For this type of study formal consent is not required.

References

1. King CR, Freeman D, Kaplan I, Fuller D, Bolzicco G, Collins S, Meier R, Wang J, Kupelian P, Steinberg M, Katz A (2013) Stereotactic body radiotherapy for localized prostate cancer: pooled analysis from a multi-institutional consortium of prospective phase II trials. Radiother Oncol 109(2):217–221
2. Fuller DB, Naitoh J, Lee C, Hardy S, Jin H (2008) Virtual HDR cyberknife treatment for localized prostatic carcinoma: dosimetry comparison with HDR brachytherapy and preliminary clinical observations. Int J Radiat Oncol Biol Phys 70(5):1588–1597
3. Schweikard A, Glosser G, Bodduluri M, Murphy MJ, Adler JR (2000) Robotic motion compensation for respiratory movement during radiosurgery. Comput Aided Surg 5(4):263–277
4. Keall PJ, Sawant A, Cho B, Ruan D, Wu J, Poulsen P, Petersen J, Newell LJ, Cattell H, Korreman S (2011) Electromagnetic-guided dynamic multileaf collimator tracking enables motion management for intensity-modulated arc therapy. Int J Radiat Oncol Biol Phys 79(1):312–320
5. Krauss A, Fast MF, Nill S, Oelfke U (2012) Multileaf collimator tracking integrated with a novel X-ray imaging system and external surrogate monitoring. Phys Med Biol 57(8):2425–2439
6. Lang S, Zeimetz J, Ochsner G, Schmid Daners M, Riesterer O, Klöck S (2014) Development and evaluation of a prototype tracking system using the treatment couch. Med Phys 41(2):021720
7. D'Souza WD, Naqvi SA, Yu CX (2005) Real-time intra-fraction-motion tracking using the treatment couch: a feasibility study. Phys Med Biol 50(17):4021–4033
8. Depuydt T, Poels K, Verellen D, Engels B, Collen C, Haverbeke C, Gevaert T, Buls N, Van Gompel G, Reynders T, Duchateau M, Tournel K, Boussaer M, Steenbeke F, Vandenbroucke F, De Ridder M (2013) Initial assessment of tumor tracking with a gimbaled linac system in clinical circumstances: a patient simulation study. Radiother Oncol 106(2):236–240
9. Tong X, Chen X, Li J, Xu Q, Lin MH, Chen L, Price RA, Ma CM (2015) Intrafractional prostate motion during external beam radiotherapy monitored by a real-time target localization system. J Appl Clin Med Phys 16(2):5013
10. Kupelian P, Willoughby T, Mahadevan A, Djemil T, Weinstein G, Jani S, Enke C, Solberg T, Flores N, Liu D, Beyer D, Levine L (2007) Multi-institutional clinical experience with the Calypso system in localization and continuous, real-time monitoring of the prostate gland during external radiotherapy. Int J Radiat Oncol Biol Phys 67(4):1088–1098
11. Fallone BG (2014) The rotating biplanar linac-magnetic resonance imaging system. Semin Radiat Oncol 24(3):200–202
12. Keall PJ, Barton M, Crozier S (2014) On behalf of the Australian MRI-Linac Program, including contributors from the Ingham Institute, Illawarra Cancer Care Centre, Liverpool Hospital, Stanford University, Universities of Newcastle, Queensland, Sydney, Western Sydney, and Wollongong. The Australian magnetic resonance imaging-linac program. Semin Radiat Oncol 24(3):203–206
13. Lagendijk JJ, Raaymakers BW, Raaijmakers AJ, Overweg J, Brown KJ, Kerkhof EM, van der Put RW, Hårdemark B, van Vulpen M,

van der Heide UA (2008) MRI/linac integration. Radiother Oncol 86(1):25–29
14. Bruder R, Ernst F, Schlaefer A, Schweikard A (2009) TH-C-304A-07: real-time tracking of the pulmonary veins in 3D ultrasound of the beating heart. 51st Annual meeting of the AAPM. Med Phys, vol 36, p 2804
15. Bruder R, Ernst F, Schlaefer A, Schweikard A (2011) A framework for real-time target tracking in radiosurgery using three-dimensional ultrasound. In: Proceedings of the 25th international congress and exhibition on computer assisted radiology and surgery (CARS'11), Int J CARS, vol 6, pp S306–S307
16. Schlosser J, Salisbury K, Hristov D (2010) Telerobotic system concept for real-time soft-tissue imaging during radiotherapy beam delivery. Med Phys 37(12):6357–6367
17. Bohrer M, Schröder P, Welzel G, Wertz H, Lohr F, Wenz F, Mai SK (2008) Reduced rectal toxicity with ultrasound-based image guided radiotherapy using BAT (B-mode acquisition and targeting system) for prostate cancer. Strahlenther Onkol 184(12):674–678
18. Cury FL, Shenouda G, Souhami L, Duclos M, Faria SL, David M, Verhaegen F, Corns R, Falco T (2006) Ultrasound-based image guided radiotherapy for prostate cancer: comparison of cross-modality and intramodality methods for daily localization during external beam radiotherapy. Int J Radiat Oncol Biol Phys 66(5):1562–1567
19. Bruder R, Ernst F, Schweikard A (2011) SU-D-220-02: optimal transducer positions for 4D ultrasound guidance in cardiac IGRT. 53rd Annual meeting of the AAPM. Med Phys, vol 38, p 3390
20. Kuhlemann I, Bruder R, Ernst F, Schweikard A (2014) WEG-BRF-09: force-and image-adaptive strategies for robotised placement of 4D ultrasound probes. 56th Annual meeting of the AAPM. Med Phys, vol 41, p 523
21. Bortfeld T (2010) The number of beams in IMRT-theoretical investigations and implications for single-arc IMRT. Phys Med Biol 55(1):83–97
22. Stein J, Mohan R, Wang XH, Bortfeld T, Wu Q, Preiser K, Ling CC, Schlegel W (1997) Number and orientations of beams in intensity-modulated radiation treatments. Med Phys 24(2):149–160
23. Schlaefer A, Gill J, Schweikard A (2008) A simulation and training environment for robotic radiosurgery. Int J CARS 3:267–274
24. Echner GG, Kilby W, Lee M, Earnst E, Sayeh S, Schlaefer A, Rhein B, Dooley JR, Lang C, Blanck O, Lessard E, Maurer CR Jr, Schlegel W (2009) The design, physical properties and clinical utility of an iris collimator for robotic radiosurgery. Phys Med Biol 54(18):5359–5380
25. Schweikard A, Schlaefer A, Adler JR Jr (2006) Resampling: an optimization method for inverse planning in robotic radiosurgery. Med Phys 33(11):4005–4011
26. Schlaefer A, Schweikard A (2008) Stepwise multi-criteria optimization for robotic radiosurgery. Med Phys 35(5):2094–2103
27. Lovelock DM, Messineo AP, Cox BW, Kollmeier MA, Zelefsky MJ (2015) Continuous monitoring and intrafraction target position correction during treatment improves target coverage for patients undergoing SBRT prostate therapy. Int J Radiat Oncol Biol Phys 91(3):588–594
28. Şen HT, Lediju BMA, Zhang Y, Ding K, Wong J, Iordachita I, Kazanzides P (2015) System integration and preliminary in-vivo experiments of a robot for ultrasound guidance and monitoring during radiotherapy. In: Proceedings of the international conference on advanced robotics, 2015, pp 53–59
29. Bazalova-Carter M, Schlosser J, Chen J, Hristov D (2015) Monte Carlo modeling of ultrasound probes for image guided radiotherapy. Med Phys 42(10):5745–5756
30. Schlosser J, Hristov D (2016) Radiolucent 4D ultrasound imaging: system design and application to radiotherapy guidance. IEEE Trans Med Imaging. doi:10.1109/TMI.2016.2559499